Accurate and Robust Reconstruction of a Surface Model of the Proximal Femur From Sparse-Point Data and a Dense-Point Distribution Model for Surgical Navigation

Guoyan Zheng*, *Member, IEEE*, Xiao Dong, Kumar T. Rajamani, Xuan Zhang, Martin Styner, Ramesh U. Thoranaghatte, Lutz-Peter Nolte, and Miguel A. González Ballester

***Abstract*—Constructing a 3-D surface model from sparse-point data is a nontrivial task. Here, we report an accurate and robust approach for reconstructing a surface model of the proximal femur from sparse-point data and a dense-point distribution model (DPDM). The problem is formulated as a three-stage optimal estimation process. The first stage, *affine registration*, is to iteratively estimate a scale and a rigid transformation between the mean surface model of the DPDM and the sparse input points. The estimation results of the first stage are used to establish point correspondences for the second stage, *statistical instantiation*, which stably instantiates a surface model from the DPDM using a statistical approach. This surface model is then fed to the third stage, *kernel-based deformation*, which further refines the surface model. Handling outliers is achieved by consistently employing the least trimmed squares (LTS) approach with a roughly estimated outlier rate in all three stages. If an optimal value of the outlier rate is preferred, we propose a hypothesis testing procedure to automatically estimate it. We present here our validations using four experiments, which include 1) leave-one-out experiment, 2) experiment on evaluating the present approach for handling pathology, 3) experiment on evaluating the present approach for handling outliers, and 4) experiment on reconstructing surface models of seven dry cadaver femurs using clinically relevant data without noise and with noise added. Our validation results demonstrate the robust performance of the present approach in handling outliers, pathology, and noise. An average 95-percentile error of 1.7–2.3 mm was found when the present approach was used to reconstruct surface models of the cadaver femurs from sparse-point data with noise added.**

***Index Terms*—Deformation, dense-point distribution model (DPDM), proximal femur, robustness, statistical instantiation.**

I. Introduction

With THE recent introduction of navigation techniques in orthopedic surgery, 3-D surface models of the patient anatomy are routinely used to provide image guidance and enhanced visualization to a surgeon to assist in planning and navigation. The common approach to derive 3-D models is to use imaging techniques such as computed tomography (CT) or magnetic resonance imaging (MRI). These have the disadvantages that they are expensive and/or induce high-radiation doses to the patient. The alternative is to reconstruct surface models using intraoperatively acquired data.

The motivation of this paper is to provide a patient-specific 3-D surface model for computer-assisted, hip surfacing surgery using intraoperatively acquired points, although the proposed approach itself can be extended to other surgical procedures such as total hip replacement and proximal femur osteotomy. Hip resurfacing surgery is considered as a very challenging procedure, even for simple cases, particularly in the accurate placement of the reaming guide wire into the femoral head. Navigation systems were proved to be helpful and promising tools in hip resurfacing, as they helped to determine several important features such as optimal component orientation, sizing, and precise positioning, and to avoid femoral notching through providing patient-specific surface models [1], [2]. The patient-specific surface model of the proximal femur in such a system reported in the literatures was either derived from a CT volume data and then registered to the patient reference coordinate system using surface points acquired through a region-based acquisition protocol [1], or generated from hundreds of intraoperatively acquired points through a surface warping [2]. The aim of this paper is to reduce the number of the points required for an accurate model generation.

However, constructing an accurate 3-D surface model from sparse data is a challenging task. Moreover, inherent to the navigation application is the high accuracy and robustness requirement. When surface reconstruction is used for the purpose of surgical guidance, it requires that the algorithm satisfies the following criteria: a) accurate geometrical information about the underlying anatomical structure can be derived from the reconstructed surface model; b) the error of the reconstructed surface model should be in the range of surgical usability, which is typically in the area of 1.5-mm average error (2 to 3 mm, worst case) as suggested by Livyatan *et al.* [3]; c) 95% success rate is normally required, when an appropriate initialization is given [3]; d) minimal user interaction during data acquisition and algorithm execution is highly appreciated for a sterilized environment; and e) the algorithm should be robust to outlying data. In

Manuscript received August 24, 2005; revised February 7, 2007. This work was supported in part by the Swiss National Science Foundation under Project NCCR CO-ME. *Asterisk indicates corresponding author.*

*G. Zheng is with the MEM Research Center, University of Bern, Stauffacherstrasse 78, CH-3014 Bern, Switzerland (e-mail: guoyan.zheng@ieee.org).

X. Dong, K. T. Rajamani, X. Zhang, R. U. Thoranaghatte, L.-P. Nolte, and M. A. González Ballester are with the MEM Research Center, University of Bern, CH-3014, Switzerland (e-mail: miguel.gonzalez@memcenter.unibe.ch).

M. Styner is with the Department of Computer Science and Psychiatry, University of North Carolina at Chapel Hill, NC 27599-7160 USA (e-mail: martin_styner@ieee.org).

Digital Object Identifier 10.1109/TBME.2007.895736

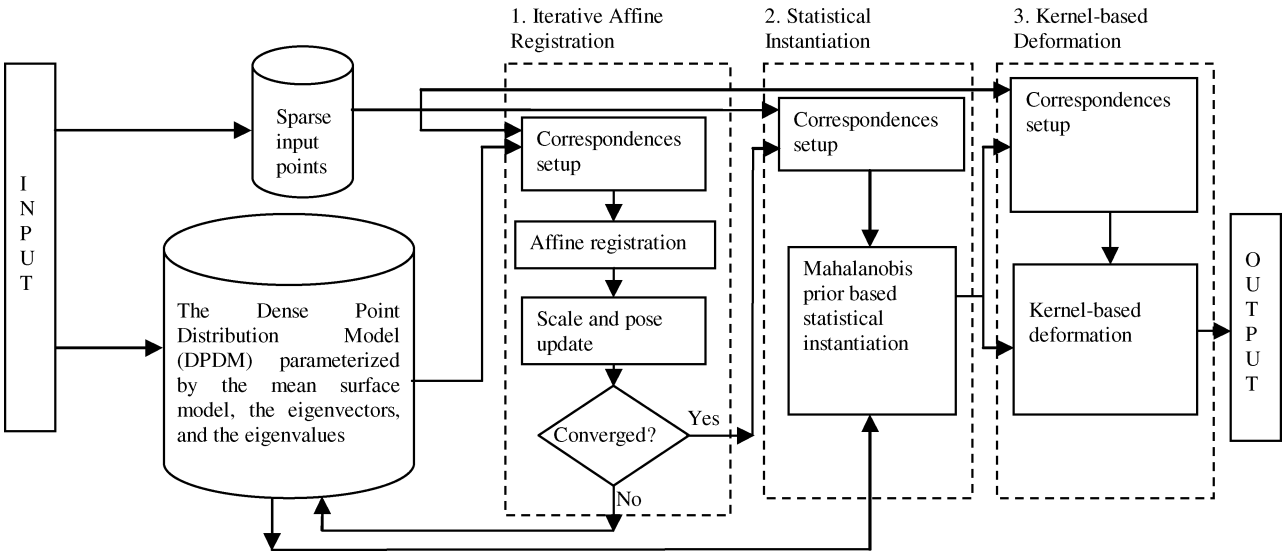

Fig. 1. Schematic diagram of the present approach. See the text for the detailed description.

this paper, we try to solve the problem in an accurate and robust way. At the heart of our approach lies the combination of sophisticated surface reconstruction techniques and a dense-point distribution model (DPDM).

The first part of this paper is to build the DPDM from a training database. A two-level approach is proposed to construct the DPDM in a fine resolution by iteratively subdividing optimally aligned surface models in a coarse resolution [4]. There are several motivations for introducing such a statistical model. First, it is treated as an important way to incorporate the *a priori* information about the shape of the target anatomical surface. Otherwise, it is a hard problem to robustly reconstruct the complete surface model from sparse data without any *a priori* information. Moreover, it facilitates the setup of point correspondences for all stages of a surface reconstruction due to its dense description [4].

The second part of this paper deals with accurately fitting the DPDM to the sparse input data [4], [5]. The fitting problem is formulated as a three-stage optimal estimation process, as shown by Fig. 1. The first stage, *affine registration*, is to iteratively estimate a scale and a rigid transformation between the mean surface model of the DPDM and the sparse input data using the iterative closest point (ICP) algorithm [6]–[8]. The estimation results of the first stage are used to establish point correspondences for the second stage, *statistical instantiation*, which stably instantiates a dense surface model from the DPDM using a Mahalanobis prior-based statistical approach [9]. This surface model is then fed to the third stage, *kernel-based deformation*. In this stage, we further refine the statistically instantiated surface model using an alternative derivation of the familiar interpolating thin-plate spline (TPS) [10] that enables weighting between the DPDM instantiated surface model and the TPS interpolation. A weighting strategy that increases the effect of the TPS interpolation as the number of input points increases is proposed.

Handling outliers is an important issue in reconstructing surface models. In this paper, it is achieved by consistently employing the least trimmed squares (LTS) approach [11] with a roughly estimated outlier rate in all three stages of the reconstruction process [5]. If an optimal value of the outlier rate is preferred, we propose a hypothesis testing procedure to automatically estimate it [5].

II. Related Works

Statistical shape analysis [12]–[14] is an important tool for understanding anatomical structures from medical images. A statistical model gives an effective parameterization of the shape variations found in a collection of sample models of a given population. Model-based approaches [15]–[17] are popular due to their ability to robustly represent objects. Intraoperative reconstruction of a patient-specific model from sparse input data can be potentially achieved through the use of a statistical model. Statistical model building consists of establishing legal variations of shape from a training population. A patient-specific model is then instantiated through fitting the statistical model to intraoperatively acquired data. Thus, the aim of the statistical instantiation is to extrapolate from sparse input data a complete and accurate anatomical representation. This is particularly interesting for minimally invasive surgery (MIS), largely due to the operating theater setup.

Several research groups have explored the methods for reconstructing a patient-specific model from a statistical model and sparse input data such as digitized points [18]–[21], a limited number of calibrated X-ray images [22]–[26], or tracked ultrasound [27]–[29]. Except for the method presented in Yao and Taylor [23], which depends on a deformable 2-D/3-D registration between an appearance-based statistical model [30] and a limited number of X-ray images, all other methods have their reliance on a point distribution model (PDM) in common. In Fleute and Lavallée [18], a statistical shape model of the distal femur was fitted to sparse input points by simultaneously optimizing both shape and pose parameters. This technology has been incorporated into a system for computer-assisted anterior cruciate ligament surgery and preliminary results were published in [19]. Chan *et al.* [27] used a similar algorithm, but optimized the shape and pose parameters separately. Tracked

ultrasound was used as the input in their work to instantiate 3-D surface models of the complete femur and pelvis from their associated statistical shape models. Cadaver study was performed to validate their method [28]. The results were compared to the associated CT-derived surface models when the latter were transformed to the patient reference coordinate system using fiducial-based registrations. It was found that the root mean square (RMS) distances between the statistically instantiated surface models and the associated CT-derived surface models were between 2.65 and 3.26 mm for the femur and around 5.0 mm for the pelvis [28]. Following the seminal work of Blanz and Vetter for the synthesis of 3-D faces using a morphable model [9], our recent work [20], [21], [29] incorporated a Mahalanobis prior for a robust and stable surface model instantiation.

Although the statistical model-based method is quite popular and has been successfully applied to different medical imaging fields such as segmenting 2-D anatomical structures [31], reconstructing surface models using digitized points [18]–[21], a limited number of calibrated X-ray images [22], [24]–[26], or tracked ultrasound [27]–[29], and reconstructing tooth surface models from sparse input data [32], the disadvantages of this method are also apparent. Using such an approach for the instantiation of a surface model is essentially equivalent to assuming that the shape variations of a given anatomy fall within a Gaussian distribution with a constant mean and covariance that are calculated from a given training database [16]. In the generative case, the law of large numbers justifies using this method [33]. Nevertheless, it may well be that part of the shape variations of a future instance can not be fully accounted for by any instance instantiated from this distribution because: a) the sparse input data may be deteriorated by noise or other errors; b) there are abnormal local shape variations due to pathology which are not modeled by the distribution; and c) shapes outside the variations of the training database can not be described by the distribution [34].

Regularization proposed in the computer vision community has also been applied to surface reconstruction from noisy measurements in a technique that defines a unique solution for these otherwise ill-posed problems by minimizing an additional smoothness functional [35]. The solutions to the minimization problems result in either implicit surface interpolations using radial basis functions [36]–[38], or variational models such as PDE-based deformable models [39], [40] or level set representations [41]–[45]. The former require either large numbers of scattered surface points as no prior information is used [36], [37], or manual interventions to find correctly the corresponding homologous features [38]. Both cases are not appropriate for our applications when taking a sterilized environment into consideration. The latter are often solved by iterations, which may be computationally very expensive. Furthermore, the stability of such iterations still remains to be solved [44].

III. Dense-Point Distribution Model Construction

We propose a two-level approach to construct the DPDM. In this work, the input data set is a training database consisting of 30 segmented proximal femur surface models from above the less trochanter. The segmentations were performed on CT volumes with a semi-automated slice by slice explicit snake algorithm [46]. Each individual surface model is described by a triangle mesh list containing 4098 vertices. A sequence of correspondence establishing methods presented in [47] was employed to optimally align these training models. It starts with a SPHARM-based parametric surface description [48] and then is optimized using minimum description length (MDL) based principle [49].

The vertices for constructing the DPDM in a fine resolution are then obtained by iteratively subdividing the aligned surface meshes in a coarse resolution. The basic idea of subdivision is to provide a smooth limit surface model which approximates the input data. Starting from a mesh in a low resolution, the limit surface model is approached by recursively tessellating the mesh. The positions of vertices created by tessellation are computed using a weighted stencil of local vertices. The complexity of the subdivision surface mesh can be increased until it satisfies the user's requirement.

In this work, we use a simple subdivision scheme called *loop scheme*, invented by Loop [50], which is based on a spline basis function, called the 3-D quartic box spline. The reasons why we choose *loop scheme* are that it is defined for triangle meshes, and that it guarantees that the limit surface mesh is smooth. Its subdivision principle is very simple. Three new vertices are inserted to divide a triangle in a coarse resolution to four smaller triangles in a fine resolution.

The levels of subdivision depend on the user's requirement. In our case, we require that the maximum edge length of all triangles should be less than 1.5 mm, which is a value determined by the average error. Given this condition, a single-level subdivision is found to be enough for our purpose.

Loop subdivision does not change the positions of vertices on the input meshes. Furthermore, positions of the inserted vertices in a fine resolution are interpolated from the neighboring vertices in a coarse resolution. As the input surface models have been optimized for establishing correspondences, it is reasonable to conclude that the output models obtained by a single-level subdivision are also aligned.

Following subdivision, the DPDM is constructed as follows. Let $\mathbf{x}_i = (p_0, p_1, \ldots, p_{N-1}),\ i = 0, 1, \ldots, m-1$ be m (here $m = 30$) members in the aligned training population. Each member is described by a vector $\mathbf{x}_i$ containing N (here, $N = 16386$) aligned 3-D point coordinates

$$\mathbf{x}_i = \{x_0, y_0, z_0, x_1, y_1, z_1, \ldots, x_{N-1}, y_{N-1}, z_{N-1}\}. \quad (1)$$

The DPDM is then constructed by applying principal component analysis (PCA) [16] on these aligned vectors as

$$\begin{aligned} \mathbf{D} &= \frac{1}{(m-1)} \cdot \sum_{i=0}^{m-1} (\mathbf{x}_i - \overline{\mathbf{x}}) \cdot (\mathbf{x}_i - \overline{\mathbf{x}})^T \\ &\quad \cdot \sigma_0 \geq \sigma_1 \geq \cdots \geq \sigma_{m'-1} > 0;\ \ m' \leq m-1 \\ \mathbf{D} \cdot \mathbf{p}_i &= \sigma_i^2 \cdot \mathbf{p}_i;\ i = 0, \ldots, m'-1 \end{aligned} \quad (2)$$

where matrices $\overline{\mathbf{x}}$ and $\mathbf{D}$ represents the mean vector and the covariance matrix, respectively; $\{\sigma_i^2\}$ are nonzero eigenvalues of

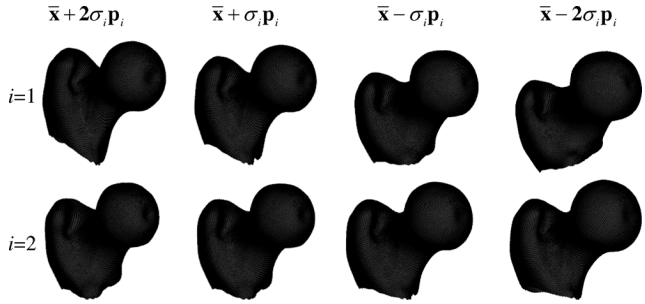

Fig. 2. First two eigenmodes of variations of our statistical shape model built from 30 segmented surface models. Each individual sample in the training database and the instantiated surface model are described by a dense triangle mesh list.

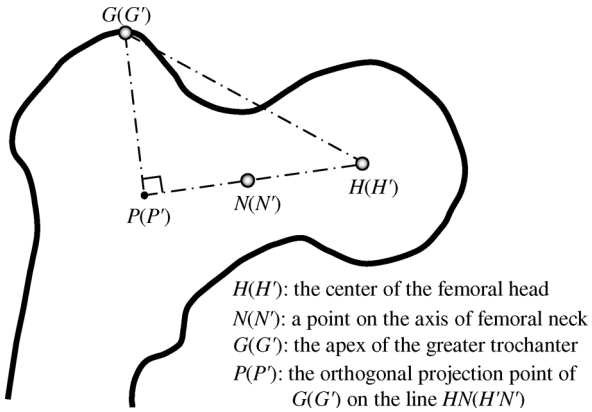

Fig. 3. Schematic view of the three anatomical landmarks used for initializing the *affine registration*.

the covariance matrix $\mathbf{D}$, and $\{\mathbf{p}_i\}$ are the corresponding eigenvectors. The sorted eigenvalues σ_i^2 and the corresponding eigenvector $\mathbf{p}_i$ of the covariance matrix are the principal directions spanning a shape space with $\overline{\mathbf{x}}$ representing its origin.

Thus, any instance $\mathbf{x}$ in this space can be described as linear combinations with weights $\boldsymbol{\alpha} = (\alpha_0, \alpha_1, \ldots, \alpha_{m'-1})^T$ calculated by projecting the vector $(\mathbf{x} - \overline{\mathbf{x}})$ into the space

$$\mathbf{x} = \overline{\mathbf{x}} + \sum_{i=0}^{m'-1} (\alpha_i \cdot \mathbf{p}_i) \tag{3}$$

and the estimated normal distribution of the coefficients $\{\alpha_i\}$ is

$$p(\alpha_0, \alpha_1, \ldots, \alpha_{m'-1}) = v_{\boldsymbol{\alpha}} \cdot e^{-1/2 \sum_{i=0}^{m'-1} (\alpha_i^2/\sigma_i^2)}$$
$$v_{\boldsymbol{\alpha}} = (2\pi)^{-m'/2} \prod_i \sigma_i^{-1} \tag{4}$$

where $\sum_{i=0}^{m'-1} (\alpha_i^2/\sigma_i^2)$ is the Mahalanobis distance from the mean according to the normal distribution.

Fig. 2 shows the variability captured by the first two modes of variations of our statistical model varied by ± 2 standard deviations.

IV. Surface Model Reconstruction Approach

Given the coordinates of a reduced number $n \ll N$ of input points in Euclidean space, $\mathbf{v}' = \{v_i' = (x_i', y_i', z_i')^T; i = 0, 1, \ldots, n-1\}$, the reconstruction problem is solved in three sequential stages: A) *affine registration*, B)*statistical instantiation*, and C) *kernel-based deformation*.

A. Affine Registration

This is a well-known problem and several efforts have been made to solve it. One of the most popular methods is the ICP algorithm developed by Besl and McKay [5], Chen and Medioni [6], and Zhang [7]. The ICP algorithm is based on the search of pairs of closest points, and the computation of a paired-point matching transformation. The resulting transformation is then applied to one set of points, and the procedure is iterated until convergence. Normally, when trying to register a set of points to a surface model described by a triangle mesh, a computation-intensive point-to-surface distance needs to be computed. However, as the mean surface model in this work is described by dense points, a cost-effective point-to-point distance is used.

It is well known that an ICP algorithm may converge to a local minimum without a proper initialization. In our case, three anatomical landmarks shown in Fig. 3, i.e., the center of the femoral head $H(H')$, a point on the axis of the femoral neck $N(N')$, and the apex of the greater trochanter $G(G')$, are used as follows to initialize the registration procedure, which guarantees the convergence of the ICP algorithm. Please note that we do not ask for a precise digitization of these landmarks, because they are just used for initialization.

Let us denote the three landmarks on the mean surface model of the DPDM as H, N, and G, and their corresponding landmarks on the anatomy as H', N', and G', respectively. H', N', and G' can be obtained intraoperatively, either by point digitization (for point G') followed by least-squares-based geometric fitting (sphere fitting for point H' and circle fitting for point N') [51], or by a pivoting algorithm (for point H') [52], or even by biplanar landmark reconstructions [53] when two or more calibrated X-ray images are used. $P'(P)$ is the orthogonal projection point of $G'(G)$ on the line $H'N'(HN)$. Let us take the point $H'(H)$ as the origin and line $N'H'(NH)$ as the $x'(x)$ axis to build a local coordinate system. The reason why we choose $H'(H)$ as the origin is that intraoperatively the point H' can be obtained more easily and more accurately than point G' and point N'. The initial scale S_0 and the initial rigid transformation (R_0, T_0) are then computed as follows:

$$\begin{cases} e_x = \frac{(P-H)}{\|P-H\|},\ e_z = \frac{PH \times GH}{\|PH \times GH\|},\ e_y = \frac{e_z \times e_x}{\|e_z \times e_x\|} \\ e'_x = \frac{(P'-H')}{\|P'-H'\|},\ e'_z = \frac{P'H' \times G'H'}{\|P'H' \times G'H'\|},\ e'_y = \frac{e'_z \times e'_x}{\|e'_z \times e'_x\|} \end{cases} \tag{5}$$

$$\begin{cases} R_1 = [\, e_x \quad e_y \quad e_z \,],\ R_2 = [\, e'_x \quad e'_y \quad e'_z \,] \\ S_0 = \sqrt{\frac{area(\Delta H'P'G')}{area(\Delta HPG)}} \\ R_0 = R_2 \cdot R_1^{-1},\ T_0 = H' - S_0 \cdot R_0 \cdot H \end{cases} \tag{6}$$

where $\times$ means to compute the cross product between two vectors, $\|\cdot\|$ means to compute the Euclidean length of a vector, and $area(\cdot)$ means to compute the area of a triangle.

B. Statistical Instantiation

After the affine registration, we can find the corresponding homologous points of the sparse input points $\mathbf{v}'$ on the dense smooth mean surface model of the DPDM. Let us denote the coordinates of these homologous points as

$$\overline{\mathbf{x}}' = C\overline{\mathbf{x}} = \{(\overline{\mathbf{x}}_j)_i; 0 \le j \le N-1;\ i = 0, 1, \ldots, n-1\} \quad (7)$$

where N is the number of points on the mean surface model of the DPDM; n is the number of the sparse input points. C represents the correspondence operation. $(\overline{\mathbf{x}}_j)_i$ denotes that the jth point $\overline{\mathbf{x}}_j$ on the mean surface model $\overline{\mathbf{x}}$ of the DPDM is the closest point to the ith input point v_i'.

Given n correspondences as well as the coordinates of these matched point pairs, our task is to estimate the coordinates of all N vertices of a complete surface model, which should have the similar shape to the mean surface model $\overline{\mathbf{x}}$ of the DPDM, and at the same time to minimize the distances between those matched point pairs. Taking these two factors into consideration, we formulate the statistical instantiation problem as the minimization of the following joint cost function [20]:

$$E_{\boldsymbol{\alpha}}(\overline{\mathbf{x}}', \mathbf{v}', \mathbf{x}) = \rho \cdot \sum_{i=0}^{n-1} \left\{ \left\| v_i' - \left[(\overline{\mathbf{x}}_j)_i + \sum_{k=0}^{m'-1} \alpha_k \cdot \mathbf{p}_k(j) \right] \right\|^2 \right\} + \sum_{k=0}^{m'-1} \left(\frac{\alpha_k^2}{\sigma_k^2} \right) \quad (8)$$

where $\{\alpha_k\}$ are the m' shape parameters that describe the to-be-instantiated surface model $\mathbf{x}$; $\mathbf{p}_k(j)$ is the jth-tuple (a 3-D vector) of the k th shape basis eigenvector.

The first term of (8) is the likelihood energy term, which measures the fitting quality of the digitized landmark sites. The second term is the prior energy term, used to penalize the deviation of the instantiated surface model from the mean surface model of the DPDM. The parameter ρ is a factor that controls the relative weighting between these two terms.

To determine each α_k, the cost function is differentiated with respect to the shape parameters and equated to zero resulting in a linear system of m' unknowns. Differentiating $E_{\boldsymbol{\alpha}}$ with respect to α_k yields

$$\frac{\partial E_{\boldsymbol{\alpha}}}{\partial \alpha_k} = \rho \cdot \sum_{i=0}^{n-1} \frac{\partial}{\partial \alpha_k} \left\{ \left\| v_i' - \left[(\overline{\mathbf{x}}_j)_i + \sum_{k=0}^{m'-1} \alpha_k \cdot \mathbf{p}_k(j) \right] \right\|^2 \right\} + \frac{2\alpha_k}{\sigma_k^2}. \quad (9)$$

E_α is differentiated with respect to each of the $\{\alpha_k\}$ and for each of the resulting equations collating the different α_k terms, and dividing throughout by 2ρ yields a linear equation system of the form $\mathbf{B} \cdot \boldsymbol{\alpha} = \mathbf{b}$ with $\mathbf{B}$ being (10), shown at the bottom of the page.

The unknowns in our system are $\boldsymbol{\alpha} = (\alpha_0, \alpha_1, \ldots, \alpha_{m'-1})^T$. Collating the constant terms yields $\mathbf{b}$, the right-hand side of the linear system

$$\sum_{i=0}^{n-1} \begin{bmatrix} [v_i' - (\overline{\mathbf{x}}_j)_i]^T \cdot \mathbf{p}_0(j) \\ \vdots \\ [v_i' - (\overline{\mathbf{x}}_j)_i]^T \cdot \mathbf{p}_k(j) \\ \vdots \\ [v_i' - (\overline{\mathbf{x}}_j)_i]^T \cdot \mathbf{p}_{m'-1}(j) \end{bmatrix}. \quad (11)$$

The parameter ρ controls the weighting between the fitting term and the prior term. It also plays an important role in determining the condition of the matrix $\mathbf{B}$ when the number of the input points is small. However, when the number of the input points increases, we would also like to put more weighting on the fitting term so that the instantiated surface model is less constrained by the Mahalanobis prior and deforms more freely to fit to the input points. Hence, the error between the instantiated surface model and the set of input points is better minimized. Since the error typically decreases exponentially when the number of digitized points increases, we choose ρ to increase logarithmically with the degree-of-freedoms (DOFs) of the input points ($= 3n$) after a certain number of points are input. It was, therefore, defined according to the following equation:

$$\rho = \begin{cases} Tr, & n \le h \\ Tr + \ln(3n - h), & n > h \end{cases} \quad (12)$$

where Tr is used to control the condition of the matrix $\mathbf{B}$ when a small number of points are digitized, h controls the starting point for the relaxation of the Mahalanobis prior constraint. After a rough theoretical analysis based on the DOFs of the DPDM ($= m'$), the first eigenvalue σ_0^2 (also the biggest eigenvalue), the number of vertices on the mean surface model ($= N$), and all the eigenvectors $\{\mathbf{p}_i\}$, Tr was set to be 0.05 and h was set to be $(m'/3)$. They were empirically found to be effective in all experiments.

When the coefficients $\boldsymbol{\alpha} = (\alpha_0, \alpha_1, \ldots, \alpha_{m'-1})^T$ are determined, the instantiated surface model is calculated by using (3).

$$\sum_{i=0}^{n-1} \begin{bmatrix} (\mathbf{p}_0(j))^T \cdot \mathbf{p}_0(j) + \frac{1}{\rho \cdot \sigma_0^2} & \cdots & (\mathbf{p}_k(j))^T \cdot \mathbf{p}_0(j) & \cdots & (\mathbf{p}_{m'-1}(j))^T \cdot \mathbf{p}_0(j) \\ \vdots & & \vdots & & \vdots \\ (\mathbf{p}_0(j))^T \cdot \mathbf{p}_k(j) & \cdots & (\mathbf{p}_k(j))^T \cdot \mathbf{p}_k(j) + \frac{1}{\rho \cdot \sigma_k^2} & \cdots & (\mathbf{p}_{m'-1}(j))^T \cdot \mathbf{p}_k(j) \\ \vdots & & \vdots & & \vdots \\ (\mathbf{p}_0(j))^T \cdot \mathbf{p}_{m'-1}(j) & \cdots & (\mathbf{p}_k(j))^T \cdot \mathbf{p}_{m'-1}(j) & \cdots & (\mathbf{p}_{m'-1}(j))^T \cdot \mathbf{p}_{m'-1}(j) + \frac{1}{\rho \cdot \sigma_{m'-1}^2} \end{bmatrix} \quad (10)$$

C. Kernel-Based Deformation

The dense surface model instantiated in the second stage is taken as the input for this stage. In this stage, we first find the corresponding homologous points of the sparse input points on the statistically instantiated surface model $\mathbf{x}$. Let us denote the coordinates of these homologous points as

$$\mathbf{v} = \{v_i = (\mathbf{x}_j)_i = (x_i, y_i, z_i)^T;\ i = 0, 1, \ldots, n-1\} \quad (13)$$

where the jth point $\mathbf{x}_j$ on the surface model $\mathbf{x}$ is the closest point to the ith input point v_i'.

To compensate for the possible positional differences between the sparse input points and their homologous points on the statistically instantiated surface model, and to estimate a nonlinear mapping $\mathbf{t} = (f, g, h)^T : \Re^3 \rightarrow \Re^3$ that describes the surface deformation (here f, g, h are the transforms of the nonlinear mapping $\mathbf{t}$ along x, y, and z direction, respectively), we formulate the deformation problem as the minimization of the following cost function:

$$E(\mathbf{t}) = \frac{1}{n} \cdot \sum_{k=0}^{n-1} [\|v_k' - \mathbf{A}v_k - \mathbf{t}(v_k)\|^2] + \tau \cdot L[\mathbf{t}] \quad (14)$$

where matrix $\mathbf{A}$ is an affine transformation to compensate for the possible positional differences between two point sets $\mathbf{v}'$ and $\mathbf{v}$. The first term of (14) measures the fitting quality. The second term, $L[\mathbf{t}] \geq 0$, is a regularization functional defined on the nonlinear mapping $\mathbf{t}$. $\tau \geq 0$ is a weighting parameter between the fitting quality and the regularization constraint.

From regularization theory [54], $L[\mathbf{t}]$ is defined as a norm in a reproducing kernel Hilbert space (RKHS) which is uniquely induced by a positive definite (or conditionally positive definite) kernel function $\phi(v_i, v_j)$. In the machine learning community, the reproducing kernels are often referred to as *Mercer kernels* [54]. They provide an elegant way of dealing with nonlinear deformation algorithms by mapping them to linear ones in some feature space nonlinearly related to the input space. Any kernel function derived from such a space can be used for our purpose. To discourage mappings that are too irregular we introduce a smoothness constraint on the deformation. One measure of the smoothness of a deformation is the space integral of the square of the second order derivatives of the nonlinear mapping. This leads us to use the familiar 3-D TPS kernel, which is conditionally positive definite and its null space is the affine subspace [10]. Now $L[\mathbf{t}]$, the measure of the smoothness of the nonlinear mapping, has the form

$$\begin{aligned} L[\mathbf{t}] &= \int\int\int_{\Re^3} (I(f) + I(g) + I(h))dxdydz \\ I(\cdot) &= \left(\frac{\partial^2}{\partial x^2}\right)^2 + 2\left(\frac{\partial^2}{\partial x \partial y}\right)^2 + \left(\frac{\partial^2}{\partial y^2}\right)^2 \\ &\quad + 2\left(\frac{\partial^2}{\partial y \partial z}\right)^2 + \left(\frac{\partial^2}{\partial z^2}\right)^2 + 2\left(\frac{\partial^2}{\partial z \partial x}\right)^2. \end{aligned} \quad (15)$$

Another advantage of using the TPS kernel is that the affine transformation $\mathbf{A}$ in (14) is automatically recovered, as components of the resultant nonlinear mapping have the form

$$\begin{cases} f(v) = a_1 + a_2 x + a_3 y + a_4 z + \sum_{i=0}^{n-1} (\gamma_i \cdot \phi(v, v_i)) \\ g(v) = b_1 + b_2 x + b_3 y + b_4 z + \sum_{i=0}^{n-1} (\theta_i \cdot \phi(v, v_i)) \\ g(v) = c_1 + c_2 x + c_3 y + c_4 z + \sum_{i=0}^{n-1} (\omega_i \cdot \phi(v, v_i)). \end{cases} \quad (16)$$

Now, the unique spatial mapping $\mathbf{t}$ that minimizes (14) comprises two matrices $\mathbf{D}$ and $\mathbf{W}$

$$E(\mathbf{t}) = \frac{1}{n} \cdot \sum_{k=0}^{n-1} \{||v_i' - [\overline{v_i} \cdot \mathbf{D} + \Phi(v_k) \cdot \mathbf{W}]^T||^2\} + \tau \cdot \mathbf{trace}(\mathbf{W}^T \mathbf{\Phi} \mathbf{W}) \quad (17)$$

where $\overline{v_i} = (1, x_i, y_i, z_i)$, $\mathbf{D} = [\mathbf{a} \quad \mathbf{b} \quad \mathbf{c}]$ is a 4×3 matrix representing the affine transformation, $\mathbf{a} = (a_1, a_2, a_3, a_4)^T$, $\mathbf{b} = (b_1, b_2, b_3, b_4)^T$, and $\mathbf{c} = (c_1, c_2, c_3, c_4)^T$ represent the affine transformation parameters along x, y, and z direction, respectively; $\Phi(v_k)$ is the kth row of the $n \times n$ symmetric matrix $\mathbf{\Phi}$, where each element $\phi_{k,i} = \|v_k - v_i\|$; $\mathbf{W} = [\boldsymbol{\gamma} \quad \boldsymbol{\theta} \quad \boldsymbol{\omega}]$ is a $n \times 3$ kernel interpolation coefficient matrix, $\boldsymbol{\gamma} = (\gamma_0, \ldots, \gamma_{n-1})^T$, $\boldsymbol{\theta} = (\theta_0, \ldots, \theta_{n-1})^T$, and $\boldsymbol{\omega} = (\omega_0, \ldots, \omega_{n-1})^T$ are the kernel interpolation coefficients along x, y, and z direction, respectively.

By taking the partial derivatives of (17) with respect to $\mathbf{D}$ and $\mathbf{W}$ and by requiring that the mapping has square integrable second derivatives [55], one obtains the linear systems of the form

$$\begin{pmatrix} (\mathbf{\Phi} + \tau \cdot \mathbf{I}) & \mathbf{P} \\ \mathbf{P}^T & \mathbf{O} \end{pmatrix} \begin{pmatrix} \boldsymbol{\gamma} & \boldsymbol{\theta} & \boldsymbol{\omega} \\ \mathbf{a} & \mathbf{b} & \mathbf{c} \end{pmatrix} = \begin{pmatrix} \mathbf{x}' & \mathbf{y}' & \mathbf{z}' \\ \mathbf{o} & \mathbf{o} & \mathbf{o} \end{pmatrix} \quad (18)$$

where $\mathbf{O}$ is a 4×4 matrix of zeros, $\mathbf{o}$ is a 4×1 column vectors of zeros, $\mathbf{P}$ is a $n \times 4$ matrix and the ith row of $\mathbf{P}$ is $(1, x_i, y_i, z_i)$, $\mathbf{x}' = (x_0', \ldots, x_{n-1}')^T$, $\mathbf{y}' = (y_0', \ldots, y_{n-1}')^T$, $\mathbf{z}' = (z_0', \ldots, z_{n-1}')^T$, $\mathbf{I}$ is a $n \times n$ identity matrix.

Following the same principle as we choose the parameter ρ, we would also like the parameter τ to enable the deformation scheme to have adaptive behavior. This is achieved by relaxing the effect of the smoothing term when the number of the input points increases. Hence, the error between the refined surface and the set of input points is better minimized. Using the same argument as we derive the parameter ρ, i.e., the error typically decreases exponentially, we choose the parameter τ to decrease logarithmically with the DOFs ($= 3n$) of the input points. It was, therefore, defined according to the following equation:

$$\tau = \frac{ce}{\ln(3n)} \quad (19)$$

where ce was empirically set to be $0.05 \cdot \ln(m')$.

The advantage of such a formulation is that it will adaptively adjust the weight for the regularization term according to the

information contained in the input data and in the training database. The reconstructed surface model is less dependent on the DPDM when more digitized points (as n becomes bigger) are added. In the extreme case when $n \to \infty$, it reduced to a pure least-squares nonlinear fitting.

V. Handling Outliers

Now assume that the input points are not outlier-free and that we can roughly estimate the value of the outlier rate; let us denote it by ξ. LTS means sorting the square errors and using a certain number of smaller values. It has been previously combined with the ICP algorithm to improve the robustness of the rigid point sets matching [56]. In this work, we propose a trimmed surface reconstruction approach for handling outliers and a procedure for automatically determining an optimal value of ξ.

A. Trimmed Surface Reconstruction Approach

The trimmed surface reconstruction approach is described as follows.

1) In each stage and for each input point, find the closest point in the associated surface model (the mean surface model of the DPDM in the first two stages, and the statistically instantiated surface model in the last stage), and compute the individual distance between them.
2) Sort all these distances in ascending order, select the $\lfloor n \cdot \xi \rfloor$ least values, where $\lfloor n \cdot \xi \rfloor$ means to compute the maximum integer that is not greater than $n \cdot \xi$.
3) Using only the $\lfloor n \cdot \xi \rfloor$ selected pairs in each stage to solve the associated equation (i.e., in the *affine registration* stage, using the $\lfloor n \cdot \xi \rfloor$ selected pairs in each iteration to estimate a scale and a rigid transformation; in the *statistical instantiation* stage, using the $\lfloor n \cdot \xi \rfloor$ selected pairs to solve (8); and in the *kernel-based deformation* stage, using the $\lfloor n \cdot \xi \rfloor$ selected pairs to solve (14).

B. Procedure for Automatically Determining an Optimal Value of the Outlier Rate

If an optimal value of ξ is preferred, one can run the trimmed surface reconstruction approach several times with a guessed outlier rate at each time, e.g., run $l+1$ times and each time use an outlier rate drawn from a set $\{\xi(i) | \xi(i) = 0.05 * i, i = 0, 1, \ldots, l\}$. The value of l is determined by the maximum outlier rate that we would like to overcome, e.g., $l = 10$ in above example for a possible maximum outlier rate of 50%. At each guessed outlier rate, the mean surface distance from the surface model estimated from the third stage to the surface model obtained from the second stage are recorded as $d(\xi(i))$. We first do a kernel smoothing by convolving the samples $d(\xi(i))$ with a kernel

$$d_l(x) = \frac{1}{l h_l} \cdot \sum_{i=0}^{l} d(\xi(i)) \cdot K\left(\frac{x - \xi(i)}{h_l}\right) \tag{20}$$

where $K(\cdot)$ is an Gaussian kernel and h_l is a bandwidth. Both of them are selected according to the standard kernel smoothing method presented in [57].

We then use a hypothesis testing procedure to check whether our input data is outlier-free or not, and if it is not, what the optimal value of the outlier rate is. The two hypotheses under consideration are as follows.

- H_0: The input data is outlier-free, we assume that $d_l(x)$ obeys a normal distribution $N(\mu_0, \sigma_0)$, where the two parameters μ_0 and σ_0 can be directly computed from $d_l(x)$.
- $H_1(p)$: The input data is not outlier-free and its outlier rate is p ($0.0 \le p \le 0.5$), we assume that the first part of $d_l(x)$ obeys a normal distribution $N(\mu_{1p}, \sigma_{1p})$ for $x \le p$ and the second part of $d_l(x)$ obeys another normal distribution $N(\mu_{2p}, \sigma_{2p})$ for $x > p$. For any given p, μ_{1p}, σ_{1p}, μ_{2p}, and σ_{2p} can be directly computed from $d_l(x)$.

Therefore, the likelihood of these two hypotheses can be calculates as

$$\begin{aligned}
&P(H_0 | d_l(x)) \\
&= \prod_{x_j \in [0.0, 0.5]} \frac{1}{\sqrt{2\pi\sigma_0^2}} \exp\left(-\frac{(d_l(x_j) - \mu_0)^2}{2\sigma_0^2}\right); j = 0, 1, \ldots, S \\
&P(H_1(p) | d_l(x)) \\
&= \prod_{x_m \in [0.0, p]} \frac{1}{\sqrt{2\pi\sigma_{1p}^2}} \exp\left(-\frac{(d_l(x_m) - \mu_{1p})^2}{2\sigma_{1p}^2}\right) \\
&\quad \cdot \prod_{x_n \in (p, 0.5]} \frac{1}{\sqrt{2\pi\sigma_{2p}^2}} \exp\left(-\frac{(d_l(x_n) - \mu_{2p})^2}{2\sigma_{2p}^2}\right) \\
&\quad m = 0, 1, \ldots, \lfloor pS \rfloor; n = \lfloor pS \rfloor + 1, \ldots, S
\end{aligned} \tag{21}$$

where S is the number of samples; x_j, x_m, and x_n are the regular sampling positions.

For any given p, we can use the log-likelihood-ratio test statistic as follows to reject H_0:

$$\Lambda(H_0, H_1(p)) = \ln \frac{\left(\frac{P(H_1(p) | d_l(x))}{P(H_0 | d_l(x))}\right)}{S}. \tag{22}$$

Then, by the optimal Neyman–Pearson test, $\Lambda(H_0, H_1(p)) > c$, provides evidence to reject H_0. The cutoff point $c = \ln(2.0)$ is selected so that the hypothesis H_0 can be correctly classified with a probability of 0.95 under the normal distribution assumptions of H_0 and $H_1(p)$.

If H_0 is rejected for at least one given p, the optimal value of the outlier rate is then estimated by finding the peak of the log-likelihood ratio. Fig. 4 gives examples of such a test for an outlier-free case [Fig. 4(a)], as well as for a case with 20% outliers [Fig. 4(b)].

VI. Experimental Results

We designed and conducted following experiments to validate the accuracy and robustness of the present approach. The accuracy depends on the shape of the given anatomy, on the number of points used for reconstruction, on the noise in the coordinates of the input points, and on whether there is pathology:

1) leave-one-out experiment;
2) experiment on evaluating the present approach for handling pathology;
3) experiment on evaluating the present approach for handling outliers;
4) experiment on reconstructing surface models of seven dry cadaver femur bones using clinically relevant data without noise and with noise added.

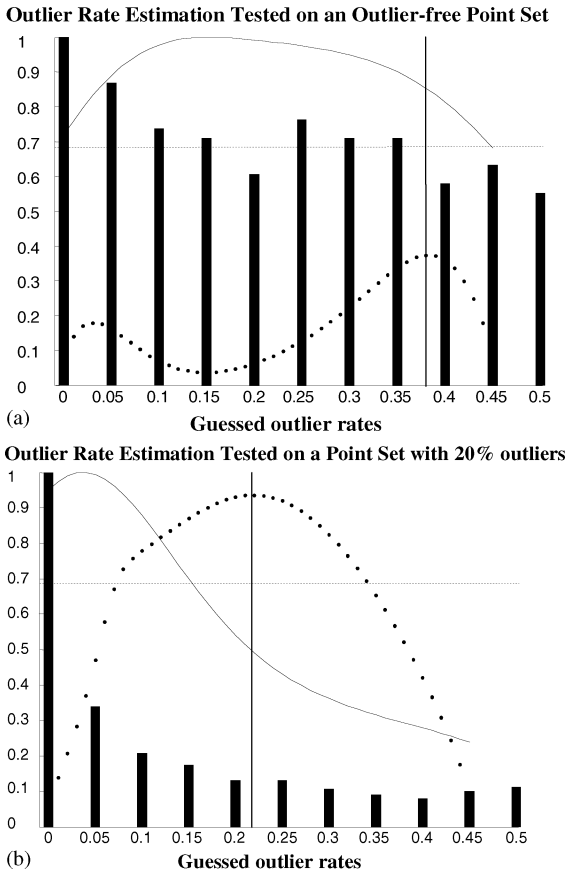

Fig. 4. Automatic estimation of an optimal value of the outlier rate using a hypothesis test procedure; (a) apply the procedure to an outlier-free case and (b) apply the procedure to a case with 20% outliers. Please keep in mind that the samples $\{d(\xi(i))\}$ in each case is normalized for better visualization. The solid curve in each figure represents the kernel smoothing results. The dotted line shows the log-likelihood ratio at different guessed outlier rates. The vertical line points out the peak of the log-likelihood ratio. The dashed line shows the cutoff point c.

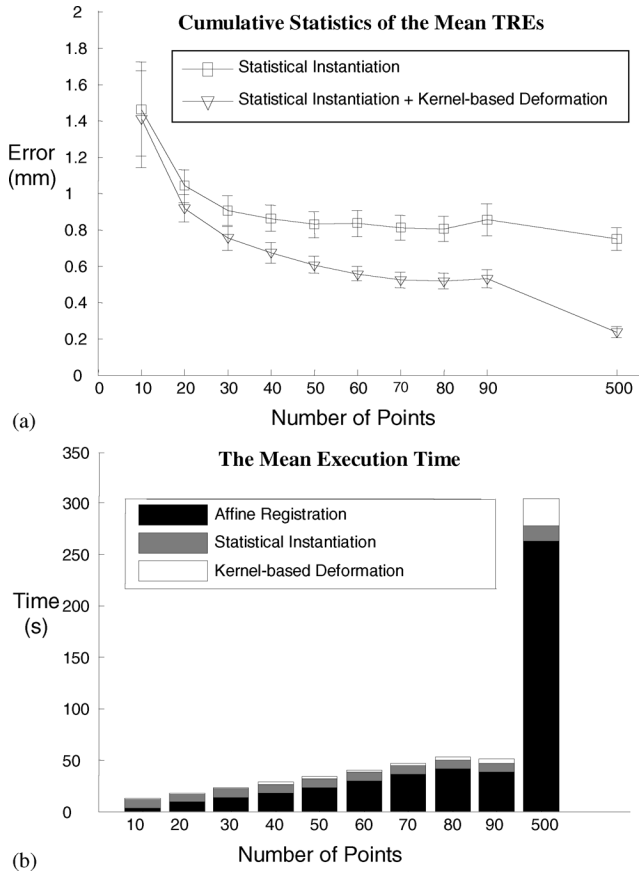

Fig. 5. Statistics cumulated from the leave-one-out experiment; (a) the cumulative mean reconstruction errors when different numbers of points were used and (b) the cumulative mean execution time when different numbers of points were used.

All experiments were performed in a Sun Blade 1000 workstation (Sun Microsystems, Mountain View, CA) with $1\times$ UltraSparc3 600-MHz CPU. The software was done using SunCC 6.2 on SunOS 5.8. Additional functionality was implemented using Qt 3.1.0 (TrollTech, Oslo, Norway). In all experiments, we propose to use target reconstruction error (TRE) to quantify the errors. TRE is defined as the distances between the actual and the reconstructed positions of selected target features, which can be landmark points or bone surfaces themselves. In the former case, TRE is obtained by first finding the closest points on the reconstructed surface model and then calculating distances between them. While in the latter case, TRE is measured by calculating the RMS distance between two discrete surface models using the open source tool *MESH* [58].

A. Leave-One-Out Experiment

A series of leave-one-out studies were carried out to evaluate the present approach. Surface points were chosen randomly from the surface model of the left-out object and were used to reconstruct the surface model of this object using the DPDM constructed from the other 29 objects. Fig. 5(a) shows the cumulative statistics from the leave-one-out studies using different number of points. Using 50 points, the cumulative mean TRE was found to be 0.8 mm when only the first two stages of the present approach were used. It decreased to 0.6 mm when all three stages were used. When more points were used, say 500 points, the difference between these two cumulative errors was more apparent (0.75 mm when only the first two stages were used versus 0.2 mm when all three stages were used). The mean execution time for each stage was also recorded and was presented as stacked bar graph in Fig. 5(b). It was found that most of the computation time was spent on the *affine registration* stage when more than 30 points were used. The leave-one-out experiment helped us evaluate the proof-of-concept of the present approach and showed that the present approach could achieve very accurate results with sparse input data and that it could seamlessly handle small and large sets of digitized points.

B. Experiment on Evaluating the Present Approach for Handling Pathology

In this experiment, we evaluated the present approach for handling pathology. The DPDM was constructed from surface models of the proximal femurs without pathology. To examine the performance of the present approach, a cadaver femur out of the training database with simulated pathology was used. The surface model derived from the CT volume data of this femur was taken as the ground truth. Points directly picked from the surface model were used for reconstruction. Fig. 6(a) shows the original surface model and the picked points. Fig. 6(b) shows the

color-coded distances between the surface model reconstructed by the statistical instantiation algorithm (i.e., the surface model output from the second stage of the present approach) and the CT-derived surface model. It was found that the distances measured around the pathological region were higher than those measured on the other regions. The color-coded distances between the surface model reconstructed by the present approach and the CT-derived surface model were presented in Fig. 6(c). The accuracy around the pathological region was significantly improved, which demonstrated the promising performance of the present approach in handling pathology.

C. Experiment on Evaluating the Present Approach for Handling Outliers

In this experiment, we evaluated the present approach for handling outliers using simulated data. The simulations were designed as follows to examine the performance of the present approach under different outlier rates. First of all, a cadaver femur which was not used in the construction of the DPDM was employed in our experiment. The surface model of this cadaver femur, which was derived from its CT volume data, was used as the ground truth; 70 points were directly picked from the surface model to create four different point sets $\{\mathbf{v}'_1, \mathbf{v}'_2, \mathbf{v}'_3, \mathbf{v}'_4\}$ with different outlier rates. $\mathbf{v}'_4$ was created by first randomly selecting 21 points from the 70 picked points, and then add a 3-D vector with a random direction whose magnitude was randomly generated from a uniform distribution in the range of 0.0 to 60.0 mm to each selected point. The outlier rate of $\mathbf{v}'_4$ is exactly 30%. By taking different numbers of outlying points and valid points out from $\mathbf{v}'_4$ we created other three point sets $\mathbf{v}'_3$, $\mathbf{v}'_2$, and $\mathbf{v}'_1$ with the exact outlier rates of 20%, 10%, and 0%, respectively. The experiment trials were then carried out in the CT coordinate system. During the reconstruction, we assumed that we had no idea whether the input point set was outlier-free or not. The approach presented in Section V was used to automatically estimate the optimal value of the outlier rate in each case. Please note that the accuracy of the outlier rate estimation depends on the density of the samples $d(\xi(i))$. The denser the samples are, the more accurate the estimation will be. However, dense samples also mean longer running time. For all studies in this experiment, each time we drew samples from the set $\{\xi(i)|\xi(i) = 0.05 * i, i = 0, 1, \ldots, l\}$. The TREs of these four studies were presented in Fig. 7(a). Fig. 7(b)–(e) shows the reconstruction example using the point set with 30% outliers. It was found that the present approach could give a proper estimate of the outlier rate in each study, i.e., 0% for $\mathbf{v}'_1$, 20% for $\mathbf{v}'_2$, 22% for $\mathbf{v}'_3$, and 25% for $\mathbf{v}'_4$, which guaranteed an accurate and robust reconstruction for each case.

D. Experiment on Reconstructing Surface Models of Seven Dry Cadaver Femurs Using Clinically Relevant Data Without Noise and With Noise Added

Finally, we demonstrated potential clinical uses of the present approach. The hip resurfacing and the total hip replacement procedures operated with the posterior approach were identified as the potential clinical applications. At one stage of such surgeries, after internal rotation and posterior dislocation of the hip, most of the femoral head, neck, and some part of trochantric and intertrochantric (crest and line) regions are exposed [59]. Obtaining sparse surface points from these intraoperatively accessible regions and reconstructing a patient-specific 3-D surface

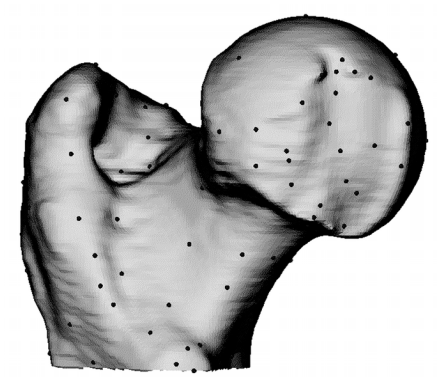

(a)

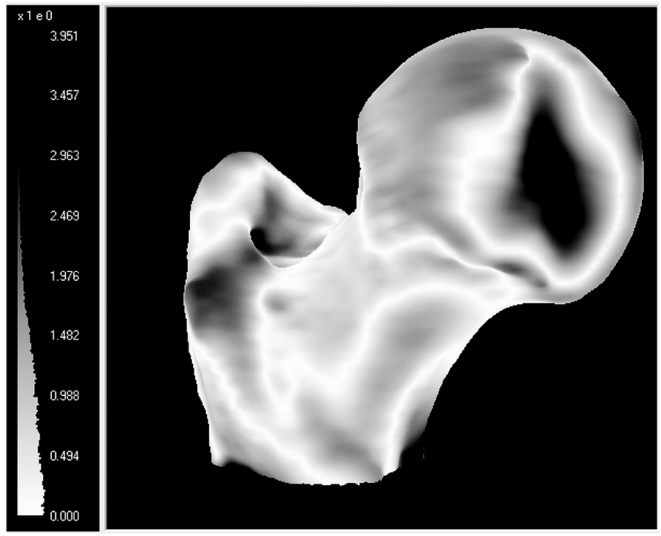

(b)

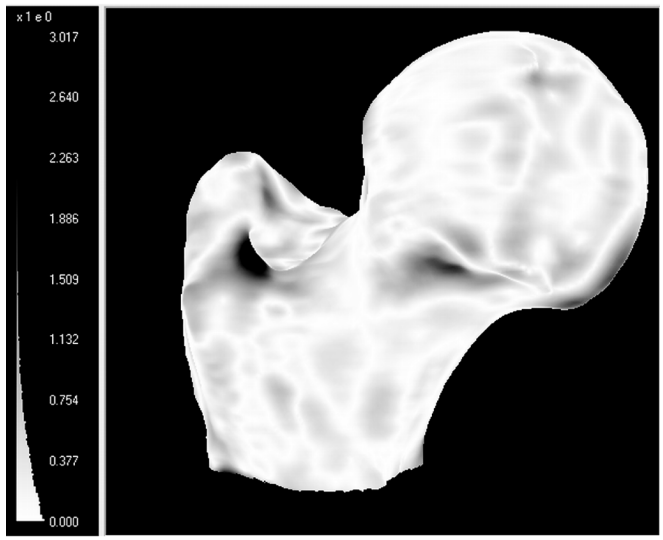

(c)

Fig. 6. Results of reconstructing a surface model of a proximal femur with simulated pathology; (a) CT-derived surface model of the bone and the digitized surface points; (b) color-coded distances between the surface model reconstructed by the statistical instantiation algorithm and the CT-derived surface model; (c) the color-coded distances between the surface model reconstructed using the present approach and the CT-derived surface model.

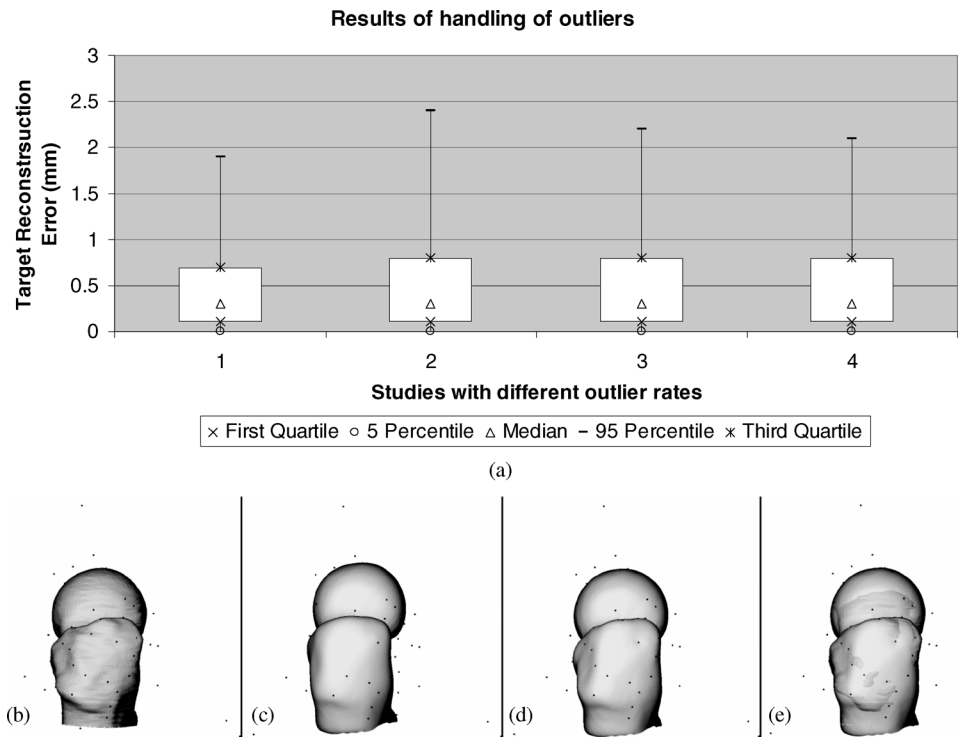

Fig. 7. Results of automatic outlier rejections. (a) TREs using the four point sets with different outlier rates; (b)–(e) reconstruction example using the point set with 30% outliers. (b) CT-derived surface model and the sparse input points with 30% outliers; (c) mean surface model and the input points; (d) reconstructed surface model and the input points; (e) reconstructed surface model, the CT-derived surface model, and the input points.

model of the proximal femur with reasonable accuracy will be useful for the above mentioned surgeries.

Seven dry cadaver femurs were used for this experiment. High-resolution CT scans of these bones were segmented and fine 3-D surface models were generated. Please note that none of these seven surface models belongs to the training database. The experiment trials were carried out in the associated CT coordinate system of each bone. For each surface model, two point sets and three anatomical landmarks were acquired. One set consisting of 50 points was used to reconstruct the surface model of the associated cadaver femur and the other set consisting of 200 points was used to evaluate the TREs. The three anatomical landmarks obtained using the method described in Section IV (point digitization followed by geometrical fittings) were used for the initialization.

The above described input data correspond to a noise-free situation. However, in a real situation, there would be errors in digitizing surface points and in finding anatomical landmarks for the initialization. To model these errors, we used the following procedure to create input data with noise added.

- To model the errors in digitizing surface points, the coordinates of the 50 picked points in each case were corrupted with additive Gaussian noise, i.e., a 3-D vector with a random direction, whose magnitude was generated from a zero mean Gaussian distribution with a certain standard deviation, was added to each picked point.
- To model the errors in finding anatomical landmarks for the initialization, the coordinates of the anatomical landmarks in each case were corrupted with additive noise, i.e., a 3-D vector with a random direction, whose magnitude was generated from a uniform distribution within a certain range, was added to the coordinates of each landmark.

In this experiment, we tested both noise-free and noise situations. Furthermore, we designed and conducted studies using two different noise conditions. In the first one, the standard deviation of the Gaussian noise was set to be 1.0 mm. The magnitude of the perturbation vector for the apex of the greater trochanter was generated from a uniform distribution within the range of 0.0 to 8.0 mm. The magnitudes of the perturbation vectors for other two landmarks were both generated from a uniform distribution within the range of 0.0 to 2.0 mm. In the second one, all other conditions were kept unchanged except that the magnitude of the perturbation vector for the apex of the greater trochanter was generated from a uniform distribution within the range of 8.0 to 15.0 mm. In both noise conditions, we repeated the procedure ten times for each case. Each time, the generated data were taken as the input to reconstruct a surface model using the present approach and various percentile errors were then calculated.

The errors of reconstructing surface models using noise-free clinically relevant data were presented in Fig. 8(a). The average errors of ten times reconstruction using clinically relevant data with noise added in two different situations were presented in Fig. 8(b) (the first condition) and Fig. 8(c) (the second condition), respectively. If we took the criterion that a reconstruction was regarded as failed when the 95-percentile error was greater than 2.5 mm, the success rates of the present approach tested in these two noise conditions were 98.6% and 87.1%, respectively. However, if we relaxed the criterion to 3.0 mm, i.e., a reconstruction was regarded as failed when the 95-percentile error was greater than 3.0 mm, then the success rates of the present approach tested in these two noise conditions would change to 100% and 98.6%, respectively. An average 95-percentile error of 1.7–2.3 mm was found when the presented ap-

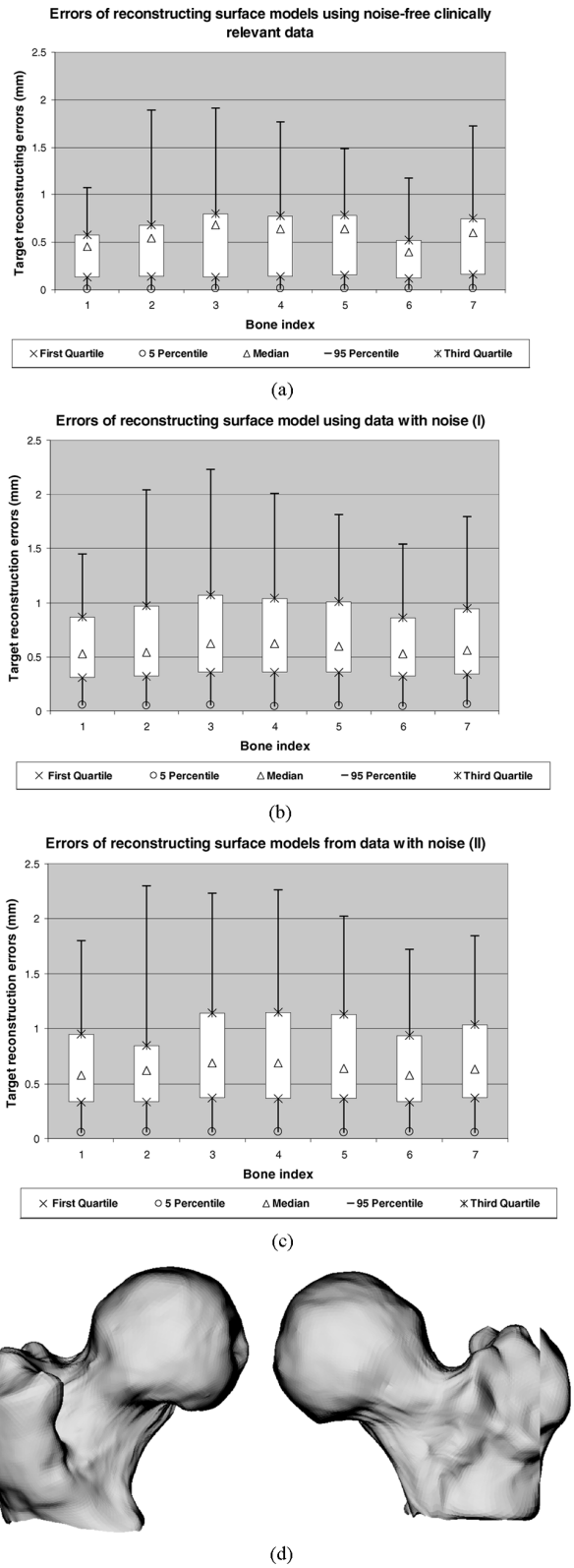

Fig. 8. Errors of reconstructing surface models of seven dry cadaver femurs using clinically relevant data without noise and with noise added; (a) TREs when noise-free clinically relevant data were used; (b) ten-times-average TREs when clinically relevant data with noise generated according to the first condition were used; (c) ten-times-average TREs when clinically relevant data with noise generated according to the second condition were used; (d) front and back views of a surface model resulted from a failed reconstruction.

proach was tested in the second noise condition. Front and back views of a surface model resulted from a failed reconstruction was presented in Fig. 8(d). Although the 95-percentile error in this case was greater then 2.5 mm, the overall shape of the proximal femur was still preserved.

VII. Discussions and Conclusion

In this paper, we have presented a robust and accurate approach to reconstruct a surface model of a given anatomy from sparse-point data and DPDM . We formulate the problem as a three-stage optimal estimation process. The optimal values of the parameters in the first stage are iteratively estimated while the optimal values of the parameters in other two stages are analytically solved. The combinations of the state-of-art reconstruction techniques and a statistical shape model as presented in our approach facilitate the accurate generation of a surface model from sparse set of surface points, which is especially attractive for minimally invasive surgery. The novel usage of the LTS approach enables for a smart estimation mechanism that is robust to outliers. Our approach can seamlessly handle small and large sets of digitized points, which is a novel concept. We have designed and conducted various experiments to show that we can robustly and accurately estimate a patient-specific 3-D surface model of the proximal femur under different conditions.

This approach is different from most of the previous works that attempt to instantiate a surface model of a given anatomy from a statistical shape model [18]–[20], [24], [27]. In addition to the statistical instantiation, we have used an additional kernel-based deformation stage to further refine the statistically instantiated surface model, which enable us to effectively handle pathology even when a statistical shape model constructed from surface models of normal anatomy is used. This has been successfully validated by our experimental results [see Fig. 6(c)], although the validation was done on one simulated pathological case. Here, we would like to give a brief explanation of how the present approach effectively handle pathology. The idea of the statistical instantiation is to instantiate a surface model from the space spanned by the eigenvectors of the covariance matrix of the training surface models, although there are different techniques to achieve it. Our formulation of the statistical instantiation problem as a Mahalanobis prior regularized least squares error minimization is one of them, which enables incorporating the complete set of eigenvectors. However, no matter what kind of statistical instantiation technique is used, such an approach is limited in their applicability to handle more complicated shape variations such as those resulted from pathology, when a statistical shape model constructed from surface models of normal anatomy is used. This has been proved by our experimental results [see Fig. 6(b)]. The idea of the kernel-based deformation presented in this work is to construct a kernel space, which is a subspace of a potentially infinite-dimensional Hilbert space induced by the TPS kernels, and to estimate a smooth deformation transform in the constructed kernel space to further refine the statistically instantiated surface model. The aims are to reduce the distances between the sparse input points and the refined surface model and at the same time to smoothly interpolate such a distance reduction effect throughout the complete surface model. The results obtained from the leave-one-out experiment and those from the experiment on handing pathology demonstrate the effectiveness of the present approach. A similar work

to ours is reported in [60], where a statistical model-based instantiation is combined with an octree splines-based local deformation to handle pathology. However, their approach requires a random cloud of as many as 1000 points. In contrast, we only need dozens of points. In addition, our formulation of the kernel-based deformation enables weighting between the statistically instantiated surface model and the TPS interpolation. The effect of the TPS interpolation is adaptively adjusted as the number of the input points increases.

There are different ways to handle outliers. It is quite easy to incorporate rectangular or box filters for outlier rejection, but they do not smartly handle the outliers and are quite rigid. Outlier resistance based on Gaussian functions seems to be an option but it suffers from slow convergence. Direct usage of M-estimators is another option but they make the minimization problem not easy to solve. The LTS approach is chosen in this work because it has better convergence rate and a smoother objective function compared to other outlier handling strategies, and more importantly, because it fits to the present approach in all three stages without any significant modification. The proposed hypothesis testing procedure enables an optimal estimation of the outlier rate, although an exact estimation of the true outlier rate is difficult. Our experimental results show that our approach can robustly reject outliers.

We have also validated the present approach using clinically relevant data without noise and with noise added. We have designed and conducted experiments to qualify the dependence of the present approach on the accurate digitization of the three anatomical landmarks for model initialization, although the possibility of digitizing these three landmarks has been confirmed by previous works [1], [2]. The success rate of the present approach depends on the accuracy of the digitization of the three anatomical landmarks for initialization. Additionally, for each failed reconstruction, we took a close look at the noise vector added to the coordinates of the apex of the greater trochanter. We found that the failed reconstructions happened when adding the noise vector caused a significant error in estimating the initial scale. Such a situation could happen in our simulation experiments but will be less likely to happen in a real situation.

The results that we have achieved in our different experiments show great promise for the potential of our approach to be applicable in clinical settings. Our carefully simulated experiments mimicking clinical settings make our technique readily usable in hip resurfacing and other related orthopedic applications. The accuracy and the success rate that we have achieved demonstrate that the present approach is appropriate for surgical navigation applications. The proposed technology can bring a variety of advantages to hip resurfacing and other surgical procedures, such as improved accuracy and safety, often reduced radiation exposure, and improved surgical reality. Our on-going work focuses on developing an accurate and robust method for reconstructing a surface model of the proximal femur from a limited number of calibrated fluoroscopic images [61]. Currently, we are evaluating the robustness and accuracy of an automatic contour extraction algorithm using data from patients and preliminary results evaluated on images from three patients is reported in [62].

ACKNOWLEDGMENT

The authors would like to thank P. Thistlethwaite and F. Langlotz for their kind help during the preparation of this paper. They would also like to thank the anonymous reviewers whose comments and suggestions helped improve the original manuscript.

REFERENCES

[1] A. R. Barrett, B. L. Davies, M. P. Gomes, S. J. Harris, J. Henckel, M. Jakopec, F. M. Rodriguez y Baena, and J. P. Cobb, "Preoperative planning and intraoperative guidance for accurate computer-assisted minimally invasive hip resurfacing surgery," *Proc. Inst. Mech. Eng. Part H—J. Eng. Med.*, vol. 220, no. 7, pp. 759–773, 2006.

[2] T. Hess, "Image free navigation for hip resurfacing," *J. Bone Joint Surg. —Br.*, vol. 88-B, p. 441-b, 2006, SUPP III.

[3] H. Livyatan, Z. Yaniv, and L. Joskowicz, "Gradient-based 2-D/3-D rigid registration of fluoroscopic X-ray to CT," *IEEE Trans. Med. Imag.*, vol. 22, no. 11, pp. 1395–1406, Nov. 2003.

[4] G. Zheng, K. T. Rajamani, and L.-P. Nolte, "Use of a dense point distribution model in a three-stage anatomical shape reconstruction from sparse information for computer assisted orthopaedic surgery: A preliminary study," in *Proc. 7th Asian Conf. Computer Vision (ACCV), Part II*, 2006, vol. 3852, pp. 52–60.

[5] G. Zheng, X. Dong, and L.-P. Nolte, "Robust and accurate reconstruction of patient-specific 3D surface models from sparse point sets: A sequential three-stage trimmed optimization approach," in *Proc. 3rd Int. Workshop Medical Imaging and Augmented Reality (MIAR)*, 2006, vol. 4091, pp. 68–75.

[6] P. Besl and N. D. McKay, "A method for registration of 3D shapes," *IEEE Trans. Pattern Anal. Mach. Intell.*, vol. 14, no. 2, pp. 239–256, Feb. 1992.

[7] Y. Chen and G. Medioni, "Object modeling by registration of multiple range images," *Image Vis. Comput.*, vol. 10, no. 3, pp. 145–155, 1992.

[8] Z. Zhang, "Iterative point matching for registration of free-form curves and surfaces," *Int. J. Comput. Vis.*, vol. 13, no. 2, pp. 119–152, 1994.

[9] V. Blanz and T. Vetter, "A morphable model for the synthesis of 3D faces," in *Proc. 26th Annu. Conf. Computer Graphics*, 1999, pp. 187–194.

[10] F. Bookstein, "Principal warps: Thin-plate splines and the decomposition of deformations," *IEEE Trans. Pattern Anal. Mach. Intell.*, vol. PAMI-11, no. 6, pp. 567–585, Jun. 1989.

[11] P. J. Rousseeuw and B. C. van Zomeren, "Unmasking multivariate outliers and leverage points," *J. Amer. Statist. Assoc.*, vol. 85, no. 411, pp. 633–639, 1990.

[12] I. L. Dryden and K. V. Mardia, *Statistical Shape Analysis*. New York: Wiley, 1998.

[13] D. Kendall, "A survey of the statistical theory of shape," *Statist. Sci.*, vol. 4, no. 2, pp. 87–99, 1989.

[14] C. Small, *The statistical Theory of Shape*. New York: Springer, 1996.

[15] M. Turk and A. Pentland, "Eigenfaces for recognition," *J. Cogn. Neurosci.*, vol. 3, no. 1, pp. 71–86, 1991.

[16] T. F. Cootes, C. J. Taylor, D. H. Cooper, and J. Graham, "Active shape models—Their training and application," *Comput. Vis. Image Understand.*, vol. 61, no. 1, pp. 38–59, 1995.

[17] I. Corouge, P. Hellier, B. Gibaud, and C. Barillot, "Interindividual functional mapping: A nonlinear local approach," *Neuroimage*, vol. 19, pp. 1337–1348, 2003.

[18] M. Fleute and S. Lavallée, "Building a complete surface model from sparse data using statistical shape models: Application to computer assisted knee surgery system," in *Proc. 1st Int. Conf. Medical Image Computing and Computer-Assisted Intervention*, 1998, vol. 1496, pp. 879–887.

[19] M. Fleute, S. Lavallée, and R. Julliard, "Incorporating a statistically based shape model into a system for computer-assisted anterior cruciate ligament surgery," *Med. Image Anal.*, vol. 3, no. 3, pp. 209–222, 1999.

[20] K. T. Rajamani, M. Styner, and S. C. Joshi, "Bone model morphing for enhanced surgical visualization," in *Proc. 2004 IEEE Int. Symp. Biomedical Imaging: From Nano to Macro*, 2004, pp. 1255–1258.

[21] K. T. Rajamani, M. A. Gonzalez Ballester, L.-P. Nolte, and M. Styner, "A novel and stable approach to anatomical structure morphing for enhanced intraoperative 3D visualization," in *Proc. SPIE Medical Imaging: Visualization, Image-guided Procedures, and Display*, 2005, vol. 5744, pp. 718–725.

[22] M. Fleute and S. Lavallée, "Nonrigid 3-D/2-D registration of images using statistical models," in *Proc. 2nd Int. Conf. Medical Image Computing and Computer-Assisted Intervention*, 1999, vol. 1679, pp. 138–147.

[23] J. Yao and R. H. Taylor, "Assessing accuracy factors in deformable 2-D/3-D medical image registration using a statistical pelvis model," in *Proc. 9th IEEE Int. Conf. Computer Vision*, 2003, vol. 2, pp. 1329–1334.

[24] H. Lamecker, T. H. Wenckebach, and H.-C. Hege, "Atlas-based 3D-shape reconstruction from X-ray images," in *Proc. 18th Int. Conf. Pattern Recognition*, 2006, vol. 1, pp. 371–374.

[25] S. Benameur, M. Mignotte, S. Parent, H. Labelle, W. Skalli, and J. A. de Guise, "3D/2D registration and segmentation of scoliotic vertebrae using statistical models," *Comput. Med. Imag. Graph.*, vol. 27, pp. 321–337, 2003.

[26] S. Benameur, M. Mignotte, H. Labelle, and J. A. de Guise, "A hierarchical statistical modeling approach for the unsupervised 3-D biplanar reconstruction of the scoliotic spine," *IEEE Trans. Biomed. Eng.*, vol. 52, no. 12, pp. 2041–2057, Dec. 2005.

[27] C. S. K. Chan, P. J. Edwards, and D. J. Hawkes, "Integration of ultrasound-based registration with statistical shape models for computer-assisted orthopaedic surgery," in *Proc. SPIE Medical Imaging: Image Processing*, 2003, vol. 5032, pp. 414–424.

[28] C. S. K. Chan, D. C. Barratt, P. J. Edwards, G. P. Penney, M. Slomczykowski, T. J. Carter, and D. J. Hawkes, "Cadaver validation of the use of ultrasound for 3D model instantiation of bony anatomy in image guided orthopaedic surgery," in *Proc. 7th Int. Conf. Medical Image Computing and Computer-Assisted Intervention, Part II*, 2004, vol. 3217, pp. 397–404.

[29] H. Talib, K. T. Rajamani, J. Kowal, L.-P. Nolte, M. Styner, and M. A. Gonzalez Ballester, "A comparison study assessing the feasibility of ultrasound-initialized deformable bone models," *Comput. Aided Surg.*, vol. 10, no. 5/6, pp. 293–299, 2005.

[30] J. Yao and R. H. Taylor, "Tetrahedral mesh modeling of density data for anatomical atlases and intensity-based registration," in *Proc. 3rd Int. Conf. Medical Image Computing and Computer-Assisted Intervention*, 2000, vol. 1935, pp. 531–540.

[31] T. F. Cootes, G. J. Taylor, and J. Haslam, "The use of active shape models for locating structures in medical images," *Image Vis. Comput.*, vol. 12, no. 6, pp. 355–365, 1994.

[32] V. Blanz, A. Mehl, T. Vetter, and H.-P. Seidel, "A statistical method for robust 3D surface reconstruction from sparse data," in *Proc. 2nd Int. Symp. 3D Data Processing, Visualization, and Transmission*, 2004, vol. 00, pp. 293–300.

[33] P. Golland, W. E. L. Grimson, M. E. Shenton, and R. Kikinis, "Small sample size learning for shape analysis of anatomical structures," in *Proc. 3rd Int. Conf. Medical Image Computing and Computer-Assisted Intervention*, 2000, vol. 1935, pp. 72–82.

[34] M. R. Kaus, J. von Berg, J. Weese, W. Niessen, and V. Pekar, "Automated segmentation of the left ventricle in cardiac MRI," *Med. Image Anal.*, vol. 8, no. 3, pp. 245–254, 2004.

[35] D. Terzopoulos, "The computation of visible-surface representations," *IEEE Trans. Pattern Anal. Mach. Intell.*, vol. 10, no. 4, pp. 417–438, Apr. 1988.

[36] B. S. Morse, T. S. Yoo, D. T. Chen, P. Rheingans, and K. R. Subramanian, "Interpolating implicit surfaces from scattered surface data using compactly supported radial basis functions," in *Proc. Int. Conf. Shape Modeling Applications*, 2001, pp. 89–98.

[37] G. Turk and J. F. O'Brien, "Shape transformation using variational implicit functions," in *Proc. 26th Annu. Conf. Computer Graphics*, 1999, pp. 335–342.

[38] R. J. A. Lapeer and R. W. Prager, "3D shape recovery of a newborn skull using thin-plate splines," *Comput. Med. Imag. Graph.*, vol. 24, no. 3, pp. 193–204, 2000.

[39] T. McInerney and D. Terzopoulos, "A finite element model for 3D shape reconstruction and nonrigid motion tracking," in *Proc. 4th Int. Conf. Computer Vision*, Berlin, Germany, May 1993, pp. 518–523.

[40] Y. Duan, L. Yang, H. Qin, and D. Samaras, "Shape reconstruction from 3D and 2D data using PDE-based deformable surfaces," in *Proc. 8th Eur. Conf. Computer Vision, Part III*, 2004, vol. 3023, pp. 238–251.

[41] S. Osher and J. A. Sethian, "Fronts propagating with curvature-dependent speed: Algorithms based on hamilton-jacobi formulations," *J. Comput. Phys.*, vol. 79, no. 1, pp. 12–49, 1988.

[42] R. T. Whitaker, "A level-set approach to 3D reconstruction from range data," *Int. J. Comput. Vis.*, vol. 29, no. 3, pp. 203–231, 1998.

[43] H.-K. Zhao, S. Osher, B. Merriman, and M. Kang, "Implicit and nonparameteric shape reconstruction from unorganized data using a variational level set method," *Comput. Vis. Image Understand.*, vol. 80, no. 3, pp. 295–314, 2000.

[44] S. Wang, J. X. Ji, and Z.-P. Liang, "Landmark-based shape deformation with topology-preserving constraints," in *Proc. 9th IEEE Int. Conf. Computer Vision*, 2003, vol. 2, pp. 923–930.

[45] J. E. Solem and F. Kahl, "Surface reconstruction using learned shape models," in *Advances in Neural Information Processing Systems 17*, L. K. Saul, Y. Weiss, and L. Bottou, Eds. Cambridge, MA: MIT Press, 2005, pp. 1305–1312.

[46] J. Hug, C. Brechbühler, and G. Székely, "Tamed snake: A particle system for robust semi-automatic segmentation," in *Proc. 2nd Inf. Conf. Medical Image Computing and Computer-Assisted Intervention*, 1999, vol. 1679, pp. 116–127.

[47] M. Styner, K. T. Rajamani, L.-P. Nolte, G. Zsemlye, G. Székely, C. J. Taylor, and R. H. Davies, "Evaluation of 3D correspondence methods for modeling building," in *Proc. 18th Int. Conf. Information Processing in Medical Imaging*, 2003, vol. 2732, pp. 63–75.

[48] C. Brechbühler, G. Gerig, and O. Kübler, "Parameterization of closed surfaces for 3D shape description," *Comput. Vis. Image Understand.*, vol. 61, no. 2, pp. 154–170, 1995.

[49] R. H. Davies, C. J. Twining, T. F. Cootes, J. C. Waterton, and C. J. Taylor, "A minimal description length approach to statistical shape modeling," *IEEE Trans. Med. Imag.*, vol. 21, no. 5, pp. 525–537, May 2002.

[50] C. T. Loop, "Smooth subdivision surfaces based on triangles," M.S. thesis, Univ. Utah, Dept. Math., Salt Lake City, 1987.

[51] J. Stoer and R. Bulirsch, *Introduction to Numerical Analysis*, 3rd ed. New York: Springer-Verlag, 2002.

[52] S. J. Piazza, A. Erdemir, N. Okita, and P. R. Cavanagh, "Assessment of the functional method of hip joint center location subject to reduced range of hip motion," *J. Biomech.*, vol. 37, no. 3, pp. 349–356, 2004.

[53] R. Hofstetter, M. Slomczykowski, C. Krettek, G. Koppen, M. Sati, and L.-P. Nolte, "Computer-assisted fluoroscopy-based reduction of femoral fractures and antetorsion correction," *Comput. Aided Surg.*, vol. 5, no. 5, pp. 311–325, 2000.

[54] T. Evgeniou, M. Pontil, and T. Poggio, "Regularization networks and support vector machines," *Adv. Comput. Math.*, vol. 13, pp. 1–50, 2000.

[55] G. Donato and S. Belongie, "Approximate thin plate spline mappings," in *Proc. 7th Eur. Conf. Computer Vision, Part III*, 2002, vol. 2352, pp. 21–31.

[56] D. Chetverikov, D. Svirko, D. Stepanov, and P. Krsek, "The trimmed iterative closest point algorithm," in *Proc. 16th Int. Conf. Pattern Recognition*, 2002, vol. 3, pp. 545–548.

[57] D. W. Scott, *Multivariate Density Estimation. Theory, Practice, and Visualization*. New York: Wiley, 1992.

[58] N. Aspert, D. Santa-Cruz, and T. Ebrahimi, "MESH: Measuring errors between surfaces using the hausdorff distance," in *Proc. IEEE Int. Conf. Multimedia and Expo*, 2002, vol. 1, pp. 705–708.

[59] J. R. Moreland, "Primary total hip Arthroplasty," in *Operative Orthopaedics*, M. W. Chapman, Ed., 1st ed. Philadelphia, PA: Lippincott, 1988, vol. 1, pp. 679–693.

[60] E. Stindel, J. L. Briard, P. Merloz, S. Plaweski, F. Dubrana, C. Lefevre, and J. Troccaz, "Bone morphing: 3D morphological data for total knee Arthroplasty," *Comput. Aided Surg.*, vol. 7, pp. 156–168, 2002.

[61] G. Zheng and L.-P. Nolte, "Surface reconstruction of bone from X-ray images and point distribution model incorporating a novel method for 2D-3D correspondence," in *Proc. IEEE Computer Society Conf. Computer Vision and Pattern Recognition*, 2006, vol. 2, pp. 2237–2244.

[62] X. Dong, M. A. Gonzalez Ballester, and G. Zheng, "Automatic extraction of proximal femur contours from calibrated fluoroscopic images," presented at the IEEE Workshop on Applications of Computer Vision, Austin, TX, 2007.

Guoyan Zheng (M'05) received the B.S. and M.S. degrees in biomedical engineering from the Southern Medical University (formerly the First Military Medical University), China, in 1992 and 1995, respectively, and the Ph.D. degree in biomedical engineering from the University of Bern, Bern, Switzerland, in 2002.

He is currently a Research Scientist and a Group Leader in the Institute for Surgical Technology and Biomechanics, MEM Research Center, University of Bern. His research interests include medical image processing and analysis, statistical shape analysis, rigid and nonrigid registration, endoscopy-based tracking, and computer-assisted interventions.

Dr. Zheng is a member of the MICCAI society.

Xiao Dong received the M.S. degree from the Beijing University of Posts and Telecommunication (BUPT), China, in 1998, and the PDEng. certificate from the Eindhoven University of Technology, Eindhoven, The Netherlands, in 2002. He is currently pursuing the Ph.D. degree at the Institute for Surgical Technology and Biomechanics, MEM Research Center, University of Bern, Bern, Switzerland.

He was a Research Assistant with the Electrical Engineering Department, Eindhoven University of Technology. His work experience includes the digital signal processing in CDMA mobile communication system, wideband adaptive beamforming for the phased-array-based radio telescope, and medical image processing. He is currently working on the statistical model-based automatic identification, segmentation, and reconstruction of anatomical structures from calibrated fluoroscopic images.

Kumar T. Rajamani received the M.Tech. degree in computer science and the M.Sc. degree in mathematics, both with distinction, from the Sri Sathya Sai Institute of Higher Learning, Prasanthi Nilayam, Andra Pradesh, India, and the Ph.D. degree in biomedical engineering from the Institute for Surgical Technology and Biomechanics, MEM Research Center, University of Bern, Bern, Switzerland, in 2006.

His main field of expertise is in shape modeling, shape deformation, and statistical shape analysis. He has a good background in medical image processing, image guidance in computer-aided surgery, active shape models, segmentation, registration, feature extraction, and 2-D image mosaicing.

Xuan Zhang received the B.S. degree from the University of Science and Technology Beijing, China, in 1998, and the M.S. degree from the Institute of Automation, Chinese Academy of Sciences, China, in 2001. He is currently pursuing the Ph.D. degree in the MEM Research Center, University of Bern, Bern, Switzerland.

In 2001, he joined in Department of Computer Science, University of Geneva, Geneva, Switzerland, as a Research Assistant.

Martin Styner received the M.S. degree from the ETH Zurich, Zurich, Switzerland, in 1997, and the Ph.D. degree from the University of North Carolina (NC), Chapel Hill, in 2001.

He is a Research Assistant Professor in the Department of Computer Science, with a joint appointment in the Department of Psychiatry, UNC. His former positions include Project Leader at the Duke Image Analysis Laboratory, Duke University, Durham, NC, and Head of the Medical Image Analysis Research Group at the M. E. Müller Research Center, University of Bern, Bern, Switzerland. His main field of expertise is in medical image processing and analysis. He has an extensive background in anatomical structure and tissue segmentation, morphometry using shape analysis, modeling and atlas building, and diffusion tensor image analysis, as well as intra- and intermodality registration.

Ramesh U. Thoranaghatte received the M.B.B.S. degree from JJM Medical College, India, in 1999, and the M.S. degree from the Indian Institute of Technology (IIT), Kharagpur, in 2004. He is currently pursuing the Ph.D. degree in biomedical engineering at the University of Bern, Bern, Switzerland.

His former positions include Resident in the Department of Surgery, JSS Medical College, India; Visiting Researcher, Computer Assisted Surgery Lab, CRIM; and Scoula Superiore Sant'Anna, Pisa, Italy, where he worked on "A Prototyle System for Tele-Collaboration in Minimally Invasive Surgeries." His main field of expertise is in endoscope-based navigation for computer-assisted surgery, image processing, and augmented reality for medical applications. Apart from in-depth medical knowledge, he has extensive engineering knowledge.

Lutz-Peter Nolte received the M.Sc. and Ph.D. degrees from the Ruhr-University Bochum, Germany, in 1980 and 1983, respectively.

He is a Professor of surgical technology and biomechanics at the University of Bern, Bern, Switzerland. From 1984 to 1987, he headed the Nonlinear Shell Research Group, Institute of Mechanics, Ruhr-University Bochum, Germany, working in the field of elastic and elasto-plastic deformations of thin-walled engineering structures. From 1987 to 1990, he established the Orthopedic Research Group, Ruhr-University Bochum, focusing his work on spinal biomechanics. In 1990, he joined the Bioengineering Center, Wayne State University, Detroit, MI, as an Associate Professor of mechanical engineering. In collaboration with the Department of Neurosurgery, he extended the scope of his research to computer-aided surgery. In 1993, he took over the Orthopedic Biomechanics Division, MEM Institute for Biomechanics, University of Bern, Bern, Switzerland. Since 2001, he has been the Co-Director of the Swiss National Center for Competence in Research "Computer Aided and Image Guided Medical Interventions" (http://co-me/), located at the ETH Zurich, Switzerland. In 2002, he became the Co-Director of the MEM Research Center for Orthopedic Surgery and the Director of the Institute for Surgical Technology and Biomechanics at the Medical Faculty, University of Bern.

Miguel A. González Ballester received the Ph.D. degree from the Robotics Research Group, University of Oxford, Oxford, U.K., in 1999, in the area of medical image analysis for the study of brain morphology and its link to the aetiology of schizophrenia and multiple sclerosis.

For two years, he was with Toshiba Medical Systems, Otawara, Japan, doing research for their MRI division. In December 2001, he received a faculty position at the Epidaure (currently renamed Asclepios) Research Group, INRIA, Sophia Antipolis, France, where he worked on image registration and statistical methods for medical image analysis, until he moved to Switzerland in mid-2004. He is currently leading the Surgical Technology Division, Institute for Surgical Technology and Biomechanics, University of Bern, Bern, Switzerland, where he also heads the Medical Image Analysis Group.